Novel Electromagnetic Design for a Precision Planar Positioner Moving Over a Superimposed Concentrated-Field Magnet Matrix

Vu Huy Nguyen, *Student Member, IEEE*, and Won-jong Kim, *Senior Member, IEEE*

***Abstract*—This paper presents the electromagnetic design and force calculation of a compact multiaxis precision positioner. A six-coil single-moving-part platen moves over a superimposed concentrated-field permanent-magnet matrix. With a rectangular coil placed in the magnetic field generated by the superimposed concentrated-field magnet matrix, the force acting on the coil is calculated by volume integration based on the Lorentz force law. The distance between the long sides and that between the short sides of a rectangular coil are designed to be a half pitch and one pitch of the magnet matrix, respectively. This allows for the simplification of force generation and calculation, compact size, and light mass (0.64 kg) of the moving platen. Six coils are divided into three two-phase linear-motor armatures with 270° or 450° phase differences. The complete force–current relation for the entire platen with the six coils is derived. Experimental results are presented to verify the working principle of the positioner designed in this paper. The positioner can be employed for the stepping and scanning applications that require 3-DOF planar motions with long travel ranges in two horizontal directions and small rotational motions about the vertical axis.**

***Index Terms*—Concentrated-field magnet matrix, electromagnetic analysis, multiaxis positioner, permanent-magnet actuator, planar motor, precision motion control.**

I. Introduction

PRECISE planar positioners have been increasingly used in a large number of applications in microscale assembly and alignment, scanning probe microscopes, surface profilometers, and microelectronic assembly. Along with these, a common application of high-precision planar positioning systems is the wafer stepper/carrier in photolithography. A 2-D magnet matrix, which can be the moving or stationary part, and windings can be employed in the applications that require precise planar motions with long travel ranges in two orthogonal directions.

Asakawa introduced the first 2-D positioning device that employed a magnet matrix and a moving-coil platen [1]. Trumper *et al*. presented a design and analysis framework for surface-mounted linear motors consisting of permanent magnets and ironless current-carrying coils [2]. The superimposed concentrated-field Halbach magnet matrix [3] was introduced in [4] and [5] and used in [6]–[8], and the study presented in this paper. Chitayat provided a magnet configuration to increase peak flux density and packing density in comparison to Asakawa's magnet matrix [9]. Cho *et al*. proposed a new 2-D permanent-magnet array for planar motors [10]. In [10, Fig. 1], the authors compare the aforementioned magnet matrices.

Sawyer motor was the first variable-reluctance type of planar motors commercially available in the industry [11]. Its advantages are high speed, long travel ranges, and capability of positioning in open loop. Its drawbacks include large cogging forces and attractive forces, overheating, and challenges in manufacturing the teeth with high precision.

Cho *et al*. analyzed and designed a permanent-magnet planar motor [12], [13]. The moving part had four three-phase permanent-magnet synchronous motors. The stationary part was the magnet matrix introduced in [10]. The force constant and the back electromotive force (EMF) constant were derived. The effect of the coil position and the coil width on the back EMF was analyzed [12]. The coil size was determined from the force calculation so that, in the horizontal plane, each motor generated the force in either x- or y-direction.

A maglev planar actuator was developed by Jansen *et al*. [7]. The translator contained a Halbach magnet array. The stationary part was an array of 84 coils oriented at a 45° angle to the magnet matrix. The set of 24 adjacent energized coils changed with the position of the translator in the xy plane [7]. The advantages were long travel ranges in x and y and no wire connected to the moving part. However, the forces acting on the moving platen were distributed within the area corresponding to the adjacent energized coils. When the platen moved, the force allocation must change when two sets of energized coils are switched. The varying error torques about the horizontal x- and y-axes should have been taken into consideration.

A compact 6-DOF precision positioner was developed by Yu [8]. In this design, the single-moving-part platen moved over a superimposed Halbach magnet matrix. There were three motors with three phases per motor. As in [5], the force calculation was based on *DQ* decomposition, and the current–force relation was linear and position independent. The motors were arranged in the platen in an optimized triangular configuration.

In this paper, a novel electromagnetic design and commutation law for a 3-DOF planar positioner moving over a superimposed Halbach magnet matrix is developed and tested [14].

Manuscript received March 1, 2011; revised June 27, 2011; accepted September 8, 2011. Date of publication February 3, 2012; date of current version February 17, 2012. Paper no. TEC-00107-2011.

V. H. Nguyen was with the Texas A&M University, College Station, TX 77840 USA and is with University of Transport and Communications, Hanoi, Vietnam (e-mail: huyvu1182@gmail.com).

W.-J. Kim is with the Texas A&M University, College Station, TX 77843-3123 USA (e-mail: wjkim@tamu.edu).

Color versions of one or more of the figures in this paper are available online at http://ieeexplore.ieee.org.

Digital Object Identifier 10.1109/TEC.2011.2170173

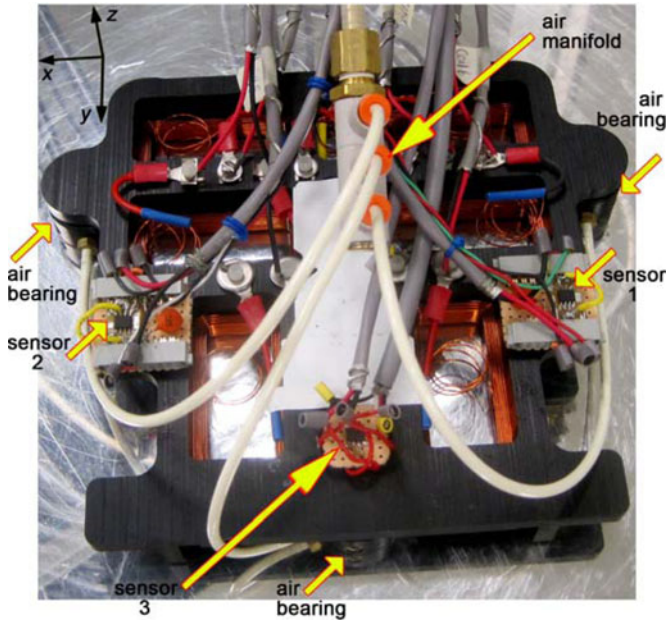

Fig. 1. Photograph of the 3-DOF planar positioner.

Fig. 1 shows a photograph of the fully assembled positioner. Three air bearings are used to support the moving platen against gravity, allowing for smooth motions without mechanical contact. The moving platen mainly consists of six coils on a Delrin frame. These six coils are divided into three two-phase linear-motor armatures with 270° or 450° phase differences. The coil size and arrangement were determined to target two purposes. First, the electromagnetic forces acting on the opposite sides of a rectangular coil double up or cancel out. This strengthens the resultant force in the desired direction and simplifies the force calculation. Second, in the horizontal plane, only one, either x or y, force component is to be generated by each motor. The disadvantage of this structure is the power cables and sensor wires connected to the moving platen, causing force disturbances. However, the significant advantages are the smallest number of coils, light mass, compact size, and low power consumption. Assuming negligible vertical motion due to very high stiffness of the air bearings, the linear current–force relation can be computed and processed in real time.

Section II derives the field solution of the concentrated-field Halbach magnet matrix by superimposing those of two single-axis Halbach magnet arrays. Section III presents the electromagnetic design of the positioner, including the analysis for coil design and placement on the moving platen. In Section IV, the electromagnetic forces acting on a single coil and the resultant electromagnetic forces acting on the 6-coil platen are calculated. Experimental results are presented in Section V.

II. Field Solution for the Superimposed Halbach Magnet Matrix

We consider a single-axis Halbach magnet array that has magnetic flux-density components in y and z [2], as shown in

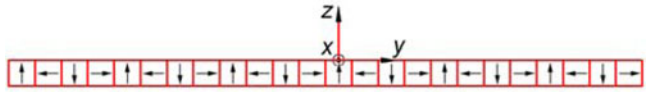

Fig. 2. Single y-axis Halbach magnet array with its magnetization.

Fig. 2. Oxyz is a Cartesian inertial coordinate system fixed to the magnet array.

Along the y-axis, the magnetic flux density varies periodically with a spatial period of L. Following [5], a complex Fourier series representation is used for the field solution. The magnetic flux density $\boldsymbol{B}$ at a point (x, y, z) is

$$\begin{aligned}\boldsymbol{B} &= \sum_{n=-\infty}^{+\infty} (B_{z,n}\boldsymbol{i}_z + B_{y,n}\boldsymbol{i}_y) \\ &= \sum_{n=-\infty}^{+\infty} (\tilde{B}_{z,n}e^{-jk_n y}\boldsymbol{i}_z + \tilde{B}_{y,n}e^{-jk_n y}\boldsymbol{i}_y). \end{aligned} \tag{1}$$

The z-component and the y-component magnetic flux densities are, respectively

$$B_z(y,z) = \sum_{n=-\infty}^{+\infty} B_{z,n}(y,z) = \sum_{n=-\infty}^{+\infty} \tilde{B}_{z,n}(y,z)e^{-jk_n y} \tag{2}$$

$$B_y(y,z) = \sum_{n=-\infty}^{+\infty} B_{y,n}(y,z) = \sum_{n=-\infty}^{+\infty} \tilde{B}_{y,n}(y,z)e^{-jk_n y} \tag{3}$$

where

$$\tilde{B}_{z,n}(y,z) = \mu_0 \left(-\frac{jk_n}{2\gamma_n}\tilde{M}_{y,n} + \frac{1}{2}\tilde{M}_{z,n}\right)(1 - e^{-\gamma_n \Delta})e^{-\gamma_n z} \tag{4}$$

$$\tilde{B}_{y,n}(y,z) = \mu_0 \left(-\frac{1}{2}\tilde{M}_{y,n} - \frac{j\gamma_n}{2k_n}\tilde{M}_{z,n}\right)(1 - e^{-\gamma_n \Delta})e^{-\gamma_n z}. \tag{5}$$

The z magnetization component is

$$\tilde{M}_{z,n} = \sqrt{2}M_0/(\pi|n|) \text{ for } n = \pm(8r+1) \text{ or } n = \pm(8r+3) \tag{6}$$

$$\tilde{M}_{z,n} = \frac{-\sqrt{2}M_0}{(\pi|n|)} \text{ for } n = \pm(8r+5) \text{ or } n = \pm(8r+7) \tag{7}$$

where r is a nonnegative integer. The y magnetization component is

$$\tilde{M}_{y,n} = j^n \tilde{M}_{z,n}. \tag{8}$$

Here, $L = 50.8$ mm is the spatial pitch of the Halbach magnet array. $k_n = 2\pi n/L$ is the spatial wave number of the nth harmonic, and $\gamma_n = |k_n|$. $\Delta = 12.7$ mm is the thickness of the magnet blocks. M_0 is their peak magnetization.

From (4) to (7), in case $n = \pm(4k+3)$, with a nonnegative integer k, we have

$$-\frac{jk_n}{2\gamma_n}\tilde{M}_{y,n} + \frac{1}{2}\tilde{M}_{z,n} = 0 \text{ and } -\frac{1}{2}\tilde{M}_{y,n} - \frac{j\gamma_n}{2k_n}\tilde{M}_{z,n} = 0. \tag{9}$$

In case $n = \pm(4k+1)$, it is clear that

$$-\frac{jk_n}{2\gamma_n}\tilde{M}_{yn} + \frac{1}{2}\tilde{M}_{zn} = \tilde{M}_{zn} \text{ and}$$

$$-\frac{1}{2}\tilde{M}_{yn} - \frac{j\gamma_n}{2k_n}\tilde{M}_{zn} = -j^n\tilde{M}_{zn}. \quad (10)$$

Therefore, for $n = 4k+1$, the following holds

$$B_{z,n}(y,z) + B_{z,-n}(y,z)$$
$$= 2\mu_0\tilde{M}_{z,n}(1-e^{-\gamma_n\Delta})e^{-\gamma_n z}\cos(k_n y)$$
$$= 2\mu_0(-1)^k\left(\frac{\sqrt{2}M_0}{\pi n}\right)(1-e^{-\gamma_n\Delta})e^{-\gamma_n z}\cos(k_n y) \quad (11)$$

$$B_{y,n}(y,z) + B_{y,-n}(y,z)$$
$$= -2\mu_0\tilde{M}_{z,n}(1-e^{-\gamma_n\Delta})e^{-\gamma_n z}\sin(k_n y)$$
$$= 2\mu_0(-1)^{k+1}\left(\frac{\sqrt{2}M_0}{\pi n}\right)(1-e^{-\gamma_n\Delta})e^{-\gamma_n z}\sin(k_n y). \quad (12)$$

The field solution for the y-axis Halbach magnet array is

$$B_{z,sg\_y}(y,z) = \sum_{k=0}^{+\infty}(-1)^k b_0(z)\cos(\gamma_n y) \quad (13)$$

$$B_{y,sg\_y}(y,z) = \sum_{k=0}^{+\infty}(-1)^{k+1} b_0(z)\sin(\gamma_n y) \quad (14)$$

where

$$b_0(z) = \frac{2\sqrt{2}\mu_0 M_0}{\pi n}(1-e^{-\gamma_n\Delta})e^{-\gamma_n z}. \quad (15)$$

Similarly, the field solution for the x-axis Halbach magnet array is

$$B_{z,sg\_x}(x,z) = \sum_{k=0}^{+\infty}(-1)^k b_0(z)\cos(\gamma_n x) \quad (16)$$

$$B_{x,sg\_x}(x,z) = \sum_{k=0}^{+\infty}(-1)^{k+1} b_0(z)\sin(\gamma_n x). \quad (17)$$

Now we consider two single-axis Halbach magnet arrays being orthogonally superimposed into a plane to yield a resultant magnetic field as shown in Fig. 3. The concept of superimposing two single Halbach magnet arrays to form a concentrated-field magnet matrix was introduced in [4], [5], and [15]. The superimposed magnet matrix comprises cubic magnet blocks and aluminum spacers. Each has the edge length of 12.7 mm. Among the magnet blocks, the ones noted as N (North) and S (South) in Fig. 4 are NdFeB50 with the remanence of 1.43 T. At their positions, two vectors of magnetic flux densities generated by the two single-axis magnet arrays are in the same direction. The magnet blocks with an arrow in Fig. 4 are NdFeB30 with the remanence of 1.10 T. At their positions, two vectors of magnetic flux densities generated by the two single-axis magnet arrays are orthogonal. The blank squares in Fig. 4 are aluminum spacers, where the magnetic flux densities generated by the two single-axis magnet arrays cancel out.

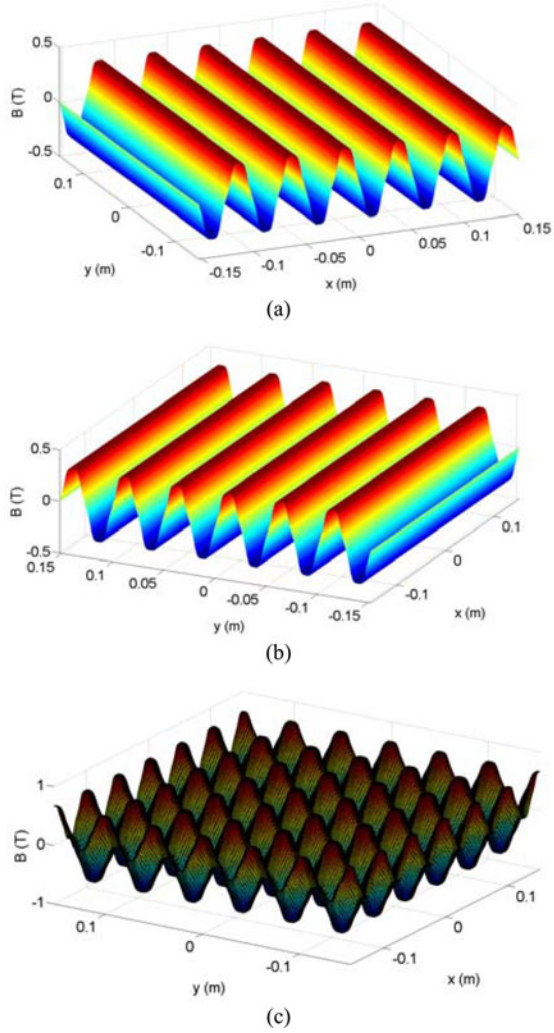

Fig. 3. Plots of (a) x-direction, (b) y-direction, and (c) z-direction magnetic flux-density components.

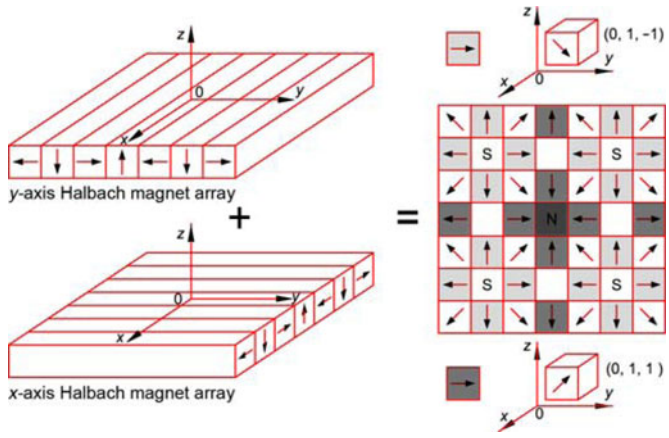

Fig. 4. Superimposing two orthogonal single-axis Habach magnet arrays.

For this superimposed Halbach magnet matrix, linear superposition holds. At every point, the resultant y- and x-direction magnetic flux-density components generated by the superimposed magnet matrix are those generated by the y-axis and

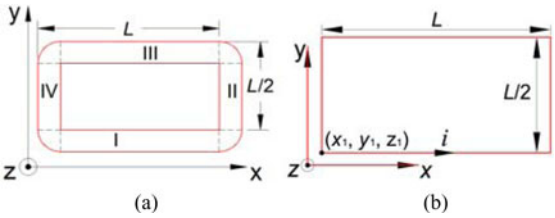

Fig. 5. (a) Dimension of the coil and (b) a single-turn coil.

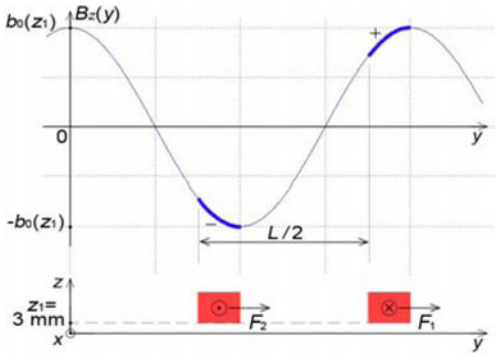

Fig. 6. Two equal forces generated by the two long coil sides.

x-axis magnet arrays, respectively. This is because the y-axis and x-axis magnet arrays do not generate the x-direction and y-direction magnetic flux-density components, respectively. The resultant z-direction magnetic flux-density component generated by the superimposed magnet matrix is the vector sum of those generated by the two single y-axis and x-axis magnet arrays, B_{z,sg_y} and B_{z,sg_x}. The field solution for the superimposed magnet matrix is

$$\begin{aligned} B_z(x,y,z) &= B_{z,sg\_y}(y,z) + B_{z,sg\_x}(x,z) \\ &= \sum_{k=0}^{+\infty} (-1)^k b_0(z)\cos(\gamma_n y) + \sum_{k=0}^{+\infty} (-1)^k b_0(z)\cos(\gamma_n x) \\ B_x(x,z) &= B_{x,sg\_x}(x,z), B_y(y,z) = B_{y,sg\_y}(y,z). \quad (18) \end{aligned}$$

Fig. 3(a)–(c), respectively, show the plots of the resultant x-, y-, and z-direction magnetic flux-density components on the plane of $z = 3$ mm.

III. Electromagnetic Design

On a plane parallel to the surface of the superimposed Halbach magnet matrix, the z-direction magnetic flux-density components B_{z,sg_x} and B_{z,sg_y} generated by the x-axis and y-axis Halbach magnet arrays vary periodically along the x-axis and the y-axis, respectively. In two opposite sides of a rectangular coil, an electric current flows in the opposite directions. We determined the dimension of a coil so that the magnetic flux densities in the two opposite sides of the coil are in reverse. In that case, the electromagnetic forces acting on these two sides add up to be stronger. For this purpose, the distance between the long sides, I and III in Fig. 5(a), of a coil is designed to be $L/2$, the half pitch of the magnet matrix. In Fig. 6, two filled rectangles are cross sections of the two long sides of a coil

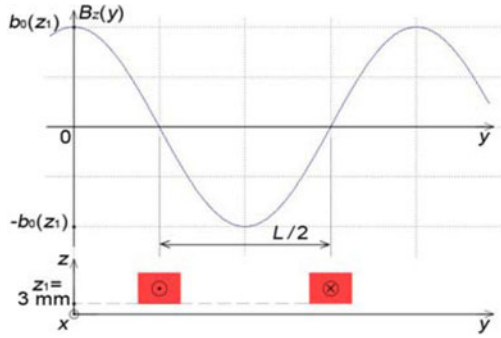

Fig. 7. Coil position where the resultant force in y is zero.

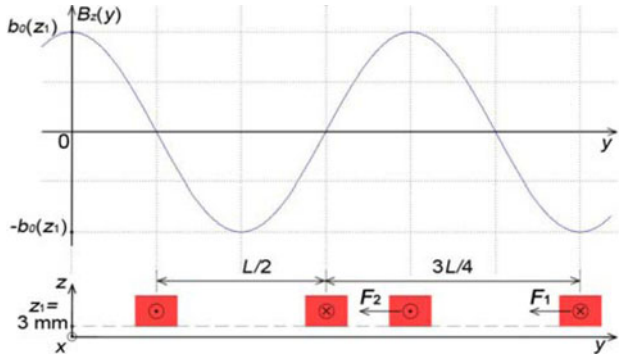

Fig. 8. Two coils complement each other to generate the resultant force in y.

with a current flowing in the opposite directions. $B_z(y)$ is the z-direction magnetic flux-density component generated by the y-axis magnet array. The two y-direction electromagnetic forces have the same magnitudes and directions.

The distance between the two short coil sides, II and IV, is designed to be L, the full pitch of the magnet matrix. The x-direction electromagnetic forces acting on sides II and IV due to the magnetic flux-density component B_{z,sg_x} have the same magnitudes and opposite directions. Thus, when considering the electromagnetic forces acting on a coil in the horizontal xy plane as in Fig. 5(a), the resultant x-direction force is zero.

For this rectangular coil, when the coil sides are aligned to the edges of the magnet matrix, there must be a position where two opposite sides are symmetric about the peak of a magnetic flux-density component. For example, in Fig. 7, the z-component magnetic flux density is distributed equally along the widths of the two coil sides. The resultant horizontal force generated by these two coil sides is zero, no matter how large the coil current is.

At least two phases are required to drive the platen in one axis. This means that for 3-DOF planar motions, the minimum number of coils needed is six. For the y-direction force component, for example, two coils are placed in parallel with a proper distance along y so that when the resultant y-direction force acting on one coil is zero, the other coil can generate the force in y. For this reason, the two coils are placed so that one leads the other by 3 $L/4$ along the y-axis. Fig. 8 illustrates this method. This set of two coils becomes a two-phase linear-motor armature with 270° phase difference. Three sets with two coils per set can

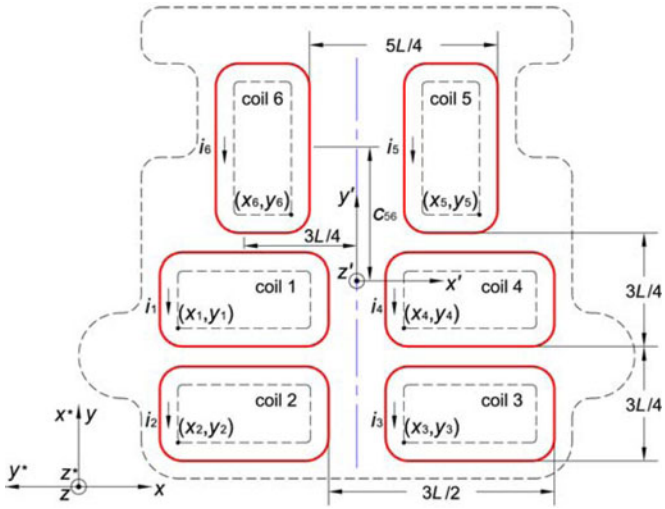

Fig. 9. Coils numbers, their relative positions, and base points.

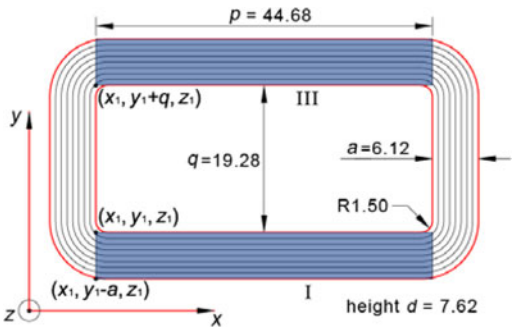

Fig. 10. Coil dimensions and the base points for force calculation, unit: mm.

generate the forces to move the platen on a plane. Fig. 9 shows the actual placement of six such coils mounted on the bottom surface of the moving platen. Instead of 270°, coils 5 and 6 as noted in Fig. 9 are separated with 450° phase difference. This is to make the mechanical design and assembly easier, providing room for an air bearing placed between coils 5 and 6.

The coil specifications were determined, and the electric currents were limited so that the displacement errors in the z-direction are negligible due to high stiffness of the air bearings, as discussed in Section IV-C. The coil dimension is given in Fig. 10. The wire type is heavy-build AWG #24 heat-bondable wire. The linear turn density of the coil along the width a is $\lambda = 1968.50$ turns/m and along the height d is $\beta = 1711.74$ turns/m. The coil resistance is 1.98 Ω, and the coil inductance is 1.28 mH by our measurements.

IV. Force Calculation and Allocation

Ignoring the four corners of a coil, we calculate the electromagnetic forces acting on four right-rectangular-prism sides of the coil by volume integration. A calculation scheme is illustrated as in Fig. 11.

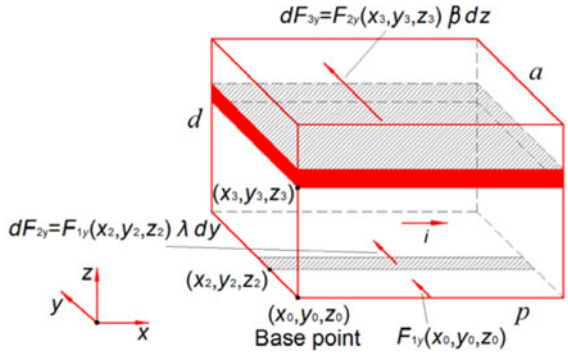

Fig. 11. Scheme to implement volume integration.

A. y-Direction Force Acting on a Right-Rectangular-Prism Coil Side

We calculate the electromagnetic force, which is generated by the resultant z-direction magnetic flux-density component, acting on a right-rectangular-prism part of the coil where the electric current flows in the positive x-direction. In all the equations throughout this paper, we use $n = 4k + 1$.

The resultant z-axis magnetic flux-density component is

$$B_z(x, y, z) = \sum_{k=0}^{+\infty} B_n(z)\cos(\gamma_n y) + \sum_{k=0}^{+\infty} B_n(z)\cos(\gamma_n x) \quad (19)$$

$$B_n(z) = (-1)^k b_0(z). \quad (20)$$

F_{3yn} is the force component acting on the coil side due to the nth-order harmonic in the expansion of $B_z(x, y, z)$, which is

$$B_{z,n} = B_n(z)\cos(\gamma_n y) + B_n(z)\cos(\gamma_n x). \quad (21)$$

The coil side has the length p along the x-axis, the width a, and the height d as shown in Fig. 11. First, we consider the force F_{1yn} acting on a line segment with length p of a single coil turn due to $B_{z,n}$. The line segment is parallel to the x-axis with the current i being flowed to the positive x-direction. $F_{1yn}(x_0, y_0, z_0)$ is the force acting on the line segment from the point (x_0, y_0, z_0) to the point $(x_0 + p, y_0, z_0)$

$$d\boldsymbol{F}_{1yn} = idx\boldsymbol{i}_x \times B_{z,n}(x, y, z)\boldsymbol{i}_z = -idxB_{z,n}(x, y, z)\boldsymbol{i}_y \quad (22)$$

$$F_{1yn}(x_0, y_0, z_0) = -i\int_{x_0}^{x_0+p} [B_n(z_0)\cos(\gamma_n y_0) + B_n(z_0)\cos(\gamma_n x)]dx$$

$$= -iB_n(z_0)\left\{p\cos(\gamma_n y_0) + \frac{2}{\gamma_n}\cos\left[\gamma_n\left(x_0 + \frac{p}{2}\right)\right]\sin\left(\frac{\gamma_n p}{2}\right)\right\}. \quad (23)$$

We denote F_{2yn} as the force due to $B_{z,n}$ acting on a rectangular cross section of the right-rectangular-prism coil side. The rectangular cross section is parallel to the xy plane and has the length p and width a. $\boldsymbol{F}_{2yn}(x_0, y_0, z_0)$ is the y-direction force

due to $B_{z,n}$ acting on the rectangular bottom surface, which contains the point (x_0, y_0, z_0), of the coil side

$$d\boldsymbol{F}_{2yn}(x,y,z) = \boldsymbol{F}_{1yn}(x,y,z)\lambda dy \tag{24}$$

$$\begin{aligned} F_{2yn}(x_0,y_0,z_0) &= \int_{y_0}^{y_0+a} F_{1yn}(x_0,y,z_0)\lambda dy \\ &= -i\lambda B_n(z_0)\int_{y_0}^{y_0+a}\left\{p\cos(\gamma_n y) \right. \\ &\qquad \left. + \frac{2}{\gamma_n}\cos\left[\gamma_n\left(x_0+\frac{p}{2}\right)\right]\sin\left(\frac{\gamma_n p}{2}\right)\right\}dy \\ &= -i\lambda B_n(z_0)\left(\frac{2}{\gamma_n}\right)\left\{p\cos\left[\gamma_n\left(y_0+\frac{a}{2}\right)\right]\sin\left(\frac{\gamma_n a}{2}\right)\right. \\ &\qquad \left. + a\cos\left[\gamma_n\left(x_0+\frac{p}{2}\right)\right]\sin\left(\frac{\gamma_n p}{2}\right)\right\}. \end{aligned} \tag{25}$$

$\boldsymbol{F}_{3yn}(x_0, y_0, z_0)$ is the resultant force due to $B_{z,n}$ acting on the right-rectangular-prism coil side with length p, width a, and height d

$$d\boldsymbol{F}_{3yn}(x,y,z) = \boldsymbol{F}_{2yn}(x,y,z)\beta dz \tag{26}$$

$$F_{3yn}(x_0,y_0,z_0) = \int_{z_0}^{z_0+d} F_{2yn}(x_0,y_0,z)\beta dz \tag{27}$$

$$\begin{aligned} F_{3yn}(x_0,y_0,z_0) &= -i\lambda\frac{2\beta}{\gamma_n}\left\{p\cos\left[\gamma_n\left(y_0+\frac{a}{2}\right)\right]\sin\left(\frac{\gamma_n a}{2}\right)\right. \\ &\quad \left. + a\cos\left[\gamma_n\left(x_0+\frac{p}{2}\right)\right]\sin\left(\frac{\gamma_n p}{2}\right)\right\}\int_{z_0}^{z_0+d} B_n(z)dz. \end{aligned} \tag{28}$$

From (15) and (20), it is seen that

$$\begin{aligned} \int_{z_0}^{z_0+d} B_n(z)dz &= (-1)^k\frac{2\sqrt{2}\mu_0 M_0}{\pi n}(1-e^{-\gamma_n\Delta})\int_{z_0}^{z_0+d} e^{-\gamma_n z}dz \\ &= \frac{(-1)^k b_0(z_0)(1-e^{-\gamma_n d})}{\gamma_n} = \frac{B_n(z_0)(1-e^{-\gamma_n d})}{\gamma_n}. \end{aligned} \tag{29}$$

From (25), (28), and (29), we have

$$F_{3yn}(x_0,y_0,z_0) = \frac{F_{2yn}(x_0,y_0,z_0)(1-e^{-\gamma_n d})\beta}{\gamma_n}. \tag{30}$$

The total y-direction electromagnetic force generated by the z-component magnetic flux density B_z acting on the coil side is found to be

$$\boldsymbol{F}_{3y} = \boldsymbol{i}_y\sum_{k=0}^{+\infty}\frac{F_{2yn}(x_0,y_0,z_0)(1-e^{-\gamma_n d})\beta}{\gamma_n}. \tag{31}$$

B. y-Direction Force Acting on a Single Coil

The resultant y-direction force acting on a single coil, as shown in Fig. 10, is the sum of two y-direction forces generated by the z-direction magnetic flux-density component of the magnet matrix, acting on the long sides I and III of the coil. The effect of quarter-cylinder parts at the corners of the coil is neglected. In practice, as in Fig. 10, at the very ends of each filled rectangles, the coil turns curve slightly with the projected length in the x-axis of the curved segments being 1.5 mm. The volume integration to calculate the force acting on each coil side is implemented with the assumption that all the segments of the coil turns along the length p of the coil side are straight lines. This approximation is reasonable for two reasons. First, it simplifies the volume integration and shortens the calculation time so that the force-current relation can be processed in real time. Second, in spite of this approximation, a feedback control loop is used to position the moving platen with the desired positioning precision.

In Fig. 10, the current flows in the sides I and III of the coil are i and $-i$, respectively. From (25) and (31), the y-direction forces due to $B_{z,n}$ acting on the sides I and III, with the base points of $(x_1, y_1 - a, z_1)$ and $(x_1, y_1 + q, z_1)$, respectively, are

$$\begin{aligned} F_{3yn}^{\mathrm{I}} &= -i\lambda\beta B_n(z_1)\left(\frac{2}{\gamma_n^2}\right)\left\{p\cos\left[\gamma_n\left(y-\frac{a}{2}\right)\right]\sin\left(\frac{\gamma_n a}{2}\right)\right. \\ &\quad \left. + a\cos\left[\gamma_n\left(x_1+\frac{p}{2}\right)\right]\sin\left(\frac{\gamma_n p}{2}\right)\right\}(1-e^{-\gamma_n d}) \end{aligned} \tag{32}$$

$$\begin{aligned} F_{3yn}^{\mathrm{III}} &= i\lambda\beta B_n(z_1)\left(\frac{2}{\gamma_n^2}\right)\left\{p\cos\left[\gamma_n\left(y_1+q+\frac{a}{2}\right)\right]\sin\left(\frac{\gamma_n a}{2}\right)\right. \\ &\quad \left. + a\cos\left[\gamma_n\left(x_1+\frac{p}{2}\right)\right]\sin\left(\frac{\gamma_n p}{2}\right)\right\}(1-e^{-\gamma_n d}). \end{aligned} \tag{33}$$

The resultant y-direction force acting on the coil is

$$F_{yn} = F_{3yn}^{\mathrm{I}} + F_{3yn}^{\mathrm{III}} = i\,b_n(z_1)\cos\left[\gamma_n\left(y_1-\frac{a}{2}\right)\right] \tag{34}$$

$$b_n(z_1) = -\lambda\beta p B_n(z_1)\left(\frac{4}{\gamma_n^2}\right)\sin\left(\frac{\gamma_n a}{2}\right)(1-e^{-\gamma_n d}). \tag{35}$$

The y-direction electromagnetic force acting on each coil side is the sum of two y-direction force components. The first one, having $\sin(\gamma_n a/2)$ in (32) and (33), is generated by the z-direction magnetic flux-density component, B_{z,sg_y}, of the single y-axis Halbach magnet array. The second force component, having $\sin(\gamma_n p/2)$ in (32) and (33), is generated by the z-direction magnetic flux-density component, B_{z,sg_x}, of the single x-axis Halbach magnet array. Because B_{z,sg_x} varies identically along the length p of the two coil sides I and III, the two y-direction electromagnetic forces acting on coil sides I and III due to B_{z,sg_x} have the same magnitude in opposite directions and are aligned in a straight line perpendicular to the x-axis. They cancel out in calculating both the resultant y-direction force and the resultant torque about the z'-axis acting on the platen. Two y-direction force components taken into account are generated by B_{z,sg_y}.

When the coil as in Fig. 10 moves along the y-axis, the y-direction force in (34) due to the n-th harmonics of $B_z(x, y, z)$ in (18) varies sinusoially with respect to y_1. The ratio between the amplitude of F_{y5}, the electromagnetic force due to the fifth-order harmonics of $B_z(x, y, z)$, and the amplitude of F_{y1}, the electromagnetic force due to the fundamental harmonics of $B_z(x, y, z)$, is calculated to be 0.950%. The ratio between the amplitude of F_{y9} and the amplitude of F_{y1} is 0.010%. Therefore, to simplify the force calculation, we only use the fundamental harmonics of the magnetic flux-density components. With (20), (34), (35), and $n = 1$, the y-direction force acting on a single

coil is

$$F_{y,\mathrm{coil}} = i\, b_1(z_1)\cos\left[\gamma_1\left(y_1 - \frac{a}{2}\right)\right] \tag{36}$$

$$b_1(z_1) = -\lambda\beta p b_0(z_1)\left(\frac{4}{\gamma_1^2}\right)\sin\left(\frac{\gamma_1 a}{2}\right)(1 - e^{-\gamma_1 d}). \tag{37}$$

With the fundamental harmonics of $B_z(x, y, z)$, the y-direction electromagnetic force acting on a single rectangular wire turn with dimensions of L in x and $L/2$ in y is

$$F_{y,\mathrm{turn}} = -2iLb_0(z_1)\cos(\gamma_1 y_1). \tag{38}$$

To validate (38), let us consider a limit case. When the coil in Fig. 10 becomes a single-turn wire as in Fig. 5(b), the thickness a and the height d of the coil approach the diameter of a single wire turn with $\lambda a \to 1$ and $\beta d \to 1$. As a and d become very small, we have $\sin(\gamma_1 a/2) \cong \gamma_1 a/2$ and $(1 - e^{-\gamma_1 d}) \cong \gamma_1 d$.

In this case, according to (37), it is seen that

$$\begin{aligned} b_1(z_1) &\cong -\lambda\beta L b_0(z_1)\left(\frac{4}{\gamma_1^2}\right)\left(\frac{\gamma_1 a}{2}\right)(\gamma_1 d) \\ &= -(\lambda a)(\beta d)2Lb_0(z_1) \to -2Lb_0(z_1). \end{aligned} \tag{39}$$

Using this result with (36), we have $F_{y,\mathrm{coil}} \cong -2iLb_0(z_1)\cos(\gamma_1 y_1)$, which matches with (38).

C. Force–Current Relation for the Six-Coil Platen

This section is to derive the transformation between the electric currents flowing in the six coils and the resultant electromagnetic forces acting on the moving platen.

1) Force Acting on the Platen in the x-Direction: The electromagnetic forces acting on the platen in the x-direction are generated by the coils 5 and 6 as shown in Fig. 9. In calculating this force, the result of Section IV-B is utilized. However, in this case, as in Fig. 9, the long sides of coils 5 and 6 are parallel to the y-axis. For coil 6, (x_1, y_1, z_1) in (36) and (37) must be replaced with $(x_6, y_6, z_1)|_{x^*y^*z^*}$ represented in the $x^*y^*z^*$ frame. In order to base on the *xyz* frame and apply (36) and (37) to calculate the x-direction electromagnetic force acting on coil 6, (x_1, y_1, z_1) in (36) and (37) is replaced by $(y_6, -x_6, z_1)|_{xyz}$, or, to be concise, $(y_6, -x_6, z_1)$. The electromagnetic force acting on coil 6 is

$$F_{x,6} = i_6 b_1(z_1)\cos\left[\gamma_1\left(x_6 + \frac{a}{2}\right)\right]. \tag{40}$$

Because $x_5 = x_6 + 5\,L/4$, for the resultant x-direction electromagnetic force acting on coil 5, x_6 in (40) is replaced with $(x_6 + 5\,L/4)$

$$F_{x,5} = -i_5 b_1(z_1)\sin\left[\gamma_1\left(x_6 + \frac{a}{2}\right)\right]. \tag{41}$$

The total force acting on the platen in the x-direction is

$$F_{x,p} = b_1(z_1)\left\{-i_5\sin\left[\gamma_1\left(x_6 + \frac{a}{2}\right)\right] + i_6\cos\left[\gamma_1\left(x_6 + \frac{a}{2}\right)\right]\right\}. \tag{42}$$

With $x_6 = x_1 + 3\,L/4$, (42) becomes

$$F_{x,p} = b_1(z_1)\left\{i_5\cos\left[\gamma_1\left(x_1 + \frac{a}{2}\right)\right] + i_6\sin\left[\gamma_1\left(x_1 + \frac{a}{2}\right)\right]\right\}. \tag{43}$$

2) Force Acting on the Platen in the y-Direction: Equations (36) and (37) can be applied directly in this case. The electromagnetic force acting on coil 1 in the y-direction is

$$F_{y,1} = i_1 b_1(z_1)\cos\left[\gamma_1\left(y_1 - \frac{a}{2}\right)\right]. \tag{44}$$

For the y-direction electromagnetic force acting on coil 2, because $y_2 = y_1 - 3\,L/4$, y_1 in (44) is replaced with $(y_1 - 3\,L/4)$.

$$F_{y,2} = -i_2 b_1(z_1)\sin\left[\gamma_1\left(y_1 - \frac{a}{2}\right)\right]. \tag{45}$$

Similarly, because $y_3 = y_1 - 3\,L/4$, the electromagnetic force acting on coil 3 in the y-direction is

$$F_{y,3} = -i_3 b_1(z_1)\sin\left[\gamma_1\left(y_1 - \frac{a}{2}\right)\right]. \tag{46}$$

Since $y_4 = y_1$, the y-direction electromagnetic force acting on coil 4 is

$$F_{y,4} = i_4\, b_1(z_1)\cos\left[\gamma_1\left(y_1 - \frac{a}{2}\right)\right]. \tag{47}$$

The resultant force acting on the platen in the y-direction is

$$\begin{aligned} F_{y,p} &= F_{y,1} + F_{y,2} + F_{y,3} + F_{y,4} \\ &= b_1(z_1)\cos\left[\gamma_1\left(y_1 - \frac{a}{2}\right)\right](i_1 + i_4) \\ &\quad - b_1(z_1)\sin\left[\gamma_1\left(y_1 - \frac{a}{2}\right)\right](i_2 + i_3). \end{aligned} \tag{48}$$

3) Torque Acting on the Platen About the z′-Axis: The torque acting on the platen about the z'-axis is generated by the horizontal electromagnetic forces acting on the coils. For coils 1, 2, 3, and 4, only the y-direction forces, which are due to B_{z,sg_y}, acting on the long coil sides contribute to the resultant torque. Projected in the x-axis, the acting points of these forces are all at the midpoints of the long coil sides

$$\begin{aligned} T_{z1234} &= T_{z1} + T_{z2} + T_{z3} + T_{z4} \\ &= \left(\frac{3L}{4}\right)(-F_{y,1} - F_{y,2} + F_{y,3} + F_{y,4}) \\ &= \left(\frac{3L}{4}\right) b_1(z_1)\cos\left[\gamma_1\left(y_1 - \frac{a}{2}\right)\right](-i_1 + i_4) \\ &\quad + \left(\frac{3L}{4}\right) b_1(z_1)\sin\left[\gamma_1\left(y_1 - \frac{a}{2}\right)\right](i_2 - i_3). \end{aligned} \tag{49}$$

For coils 5 and 6, only the x-direction forces, which are due to B_{z,sg_x}, acting on the long coil sides contribute to the resultant torque. Projected in the y-axis, the acting points of these forces are at the midpoint of the long coil sides with a distance of $c_{56} = 44.4$ mm to the center of mass of the moving platen, as described

in Fig. 9

$$T_{z56} = T_{z5} + T_{z6} = c_{56}(-F_{x,5} - F_{x,6}) = -c_{56}b_1(z_1)\left\{i_5 \cos\left[\gamma_1\left(x_1 + \frac{a}{2}\right)\right] + i_6 \sin\left[\gamma_1\left(x_1 + \frac{a}{2}\right)\right]\right\}. \quad (50)$$

The total torque acting on the platen about the z'-axis is

$$T_z = T_{z1234} + T_{z56}. \quad (51)$$

Equations (43), (48), and (51) show that the current–force relations for 3-DOF planar motions of the 6-coil platen are linear and sinusoidally position dependent. The x- and y-direction forces depend on x and y alone, respectively. A key feature is that, being projected onto the horizontal plane, the point that the resultant horizontal electromagnetic force acting on a coil is in the symmetrical axis perpendicular to the long coil sides.

4) Force Acting on the Platen in the z-Direction: The z-direction electromagnetic forces acting on coils 1 and 2 are calculated to be

$$F_{z,1} = i_1 b_1(z_1) \sin\left[\gamma_1\left(y_1 - \frac{a}{2}\right)\right] \quad (52)$$

$$F_{z,2} = i_2 b_1(z_1) \cos\left[\gamma_1\left(y_1 - \frac{a}{2}\right)\right]. \quad (53)$$

With the maximum electric current of 1 A flowing in each coil, the maximum resultant z-direction force generated by the set of coils 1 and 2 is calculated to be

$$F_{z,12\_\max} = |\sqrt{2}b_1(z_1)| = 4.4\,\text{N}. \quad (54)$$

Similarly, the maximum z-direction electromagnetic forces generated by the set of coils 3 and 4, and the set of coils 5 and 6 are calculated to be 4.4 N. With the air-bearing stiffness of 17 000 N/mm, the maximum vertical displacement of the moving platen is estimated to be 0.26 μm. The maximum rotation angles about the y'- and x'-axes are estimated as 6.8 and 7.4 μrad, respectively. Therefore, the position errors in z and in rotations about x' and y' are negligible. It is considered that the bottom surface of the moving platen is parallel to and has a uniform distance from the top surface of the magnet matrix.

D. Force Allocation for 3-DOF Planar Motions

Each of the set of coils 1 and 2 and the set of coils 3 and 4 can only generate two independent force components in the y- and z-directions. Coils 5 and 6 can only generate two independent force components in the x- and z-directions. Fig. 12 shows the force allocations to generate all three-axis motions in the xy plane. In order to move the platen in the y-direction, the set of coils 1 and 2 and the set of coils 3 and 4 generate two resultant forces in the same direction. In order to move the platen in the x-direction, coils 5 and 6 are energized to yield a resultant force in the x-direction, concurrently generating an error torque about the z'-axis. This torque must be cancelled by two forces with the same magnitude but in opposite directions generated by the set of coils 1 and 2 and the set of coils 3 and 4. For the rotations about the z'-axis, the set of coils 1 and 2 and the set of coils 3 and 4 generate two resultant forces with the same magnitude in opposite directions.

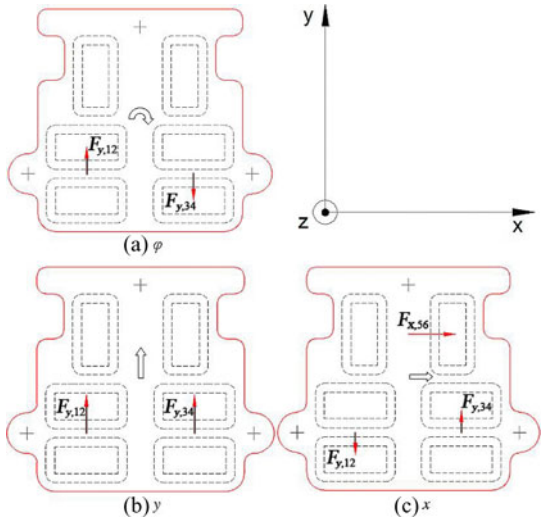

Fig. 12. Illustration of 3-DOF motion generation.

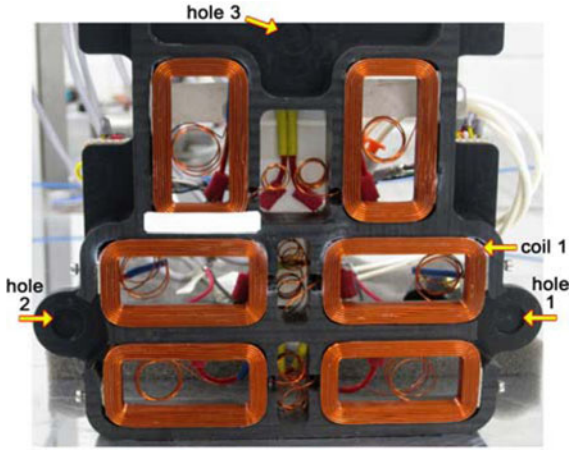

Fig. 13. Bottom view of the platen with six coils mounted.

V. Experimental Results

Fig. 13 shows the bottom view of the moving platen with the six coils mounted. Three holes are for air-bearing support. The frame of the moving platen (185.4 mm × 157.9 mm) is made of Delrin. The total mass of the moving platen is only 0.64 kg. The principal moment of inertia of the platen about the vertical axis penetrating the center of mass is $I_z = 0.001\,\text{kg}\cdot\text{m}^2$. A Versa Module Eurocand-bus instrumentation system is used for real-time digital control of the positioner. Pentek 4284 is the target DSP board with the central processing unit TMS320C40. Pentek 6102, having eight analog-to-digital and eight digital-to-analog channels with 16-bit resolution, is used as the data acquisition board. The sampling frequency is 1 kHz. The power amplifier gain is 0.506 with the bandwidth of 6.893 kHz.

Three two-axis Hall-effect sensors (the 2 SA-10 by Sentron) with their locations shown in Fig. 1 are used to measure the

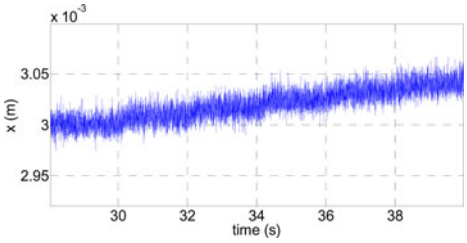

Fig 14. Five consecutive steps of 8 μm in x.

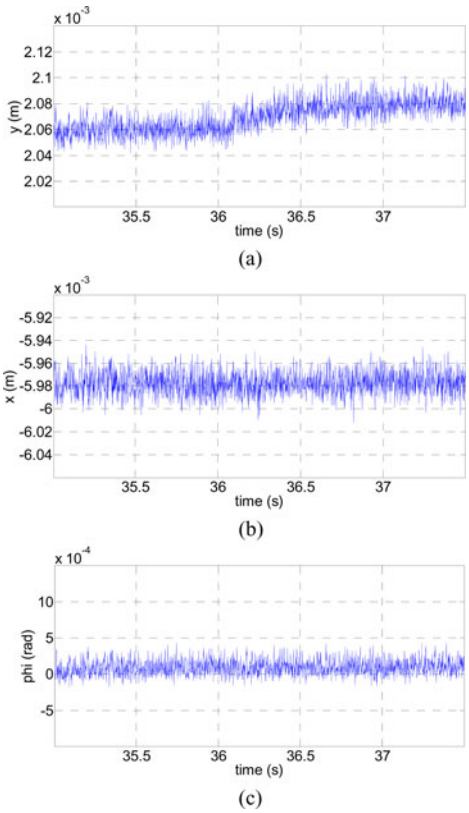

Fig. 15. (a) Step response of 20 μm in y and perturbations in (b) x and (c) φ.

magnetic flux densities generated by the magnet matrix. Each sensor is attached to the moving platen so that its sensitive directions are x' and y'. Sensors 1 and 2 are aligned along the x'-axis with a distance of 127.00 mm. The distance between sensors 1 and 3 along the y'-axis is 38.10 mm. The position of the moving platen is determined by the data measured by these sensors and the field solution derived in Section II. To determine the position of the moving platen in x or y, sensors 1 and 3 are used. To determine the platen's rotation about z', sensors 1 and 2 are used. In this system, instead of using the platen's position for feedback, the magnetic flux densities measured by the Hall-effect sensors are utilized directly.

For single-axis translational motions in x and y and small-angle rotations about z', a digital-proportional-integral-derivative-like controller was designed and implemented to verify the working principle of the electromagnetic design in this paper. We regard the six coils as three sets with two coils per set sharing a common control effort. Representative step responses are shown in Figs. 14–18. Fig. 14 shows five consecutive 8-μm steps in x. Fig. 15(a)–(c) give a step response of 20 μm in y with the rise time of 0.25 s and the perturbations in x and in rotation about z'. In Figs. 16 and 17, staircase responses in x and y

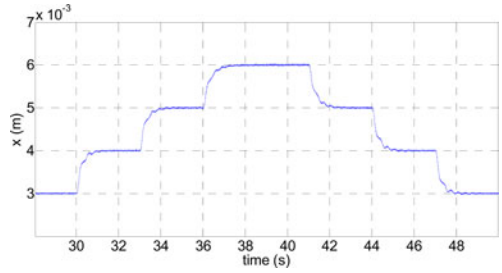

Fig. 16. Staircase response with step size of 1000 μm in x.

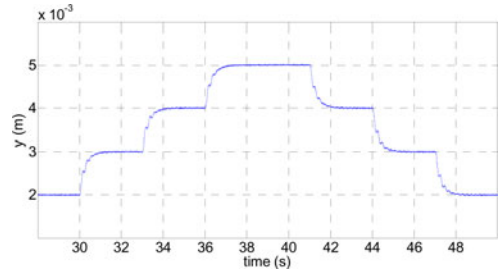

Fig. 17. Staircase response with step size of 1000 μm in y.

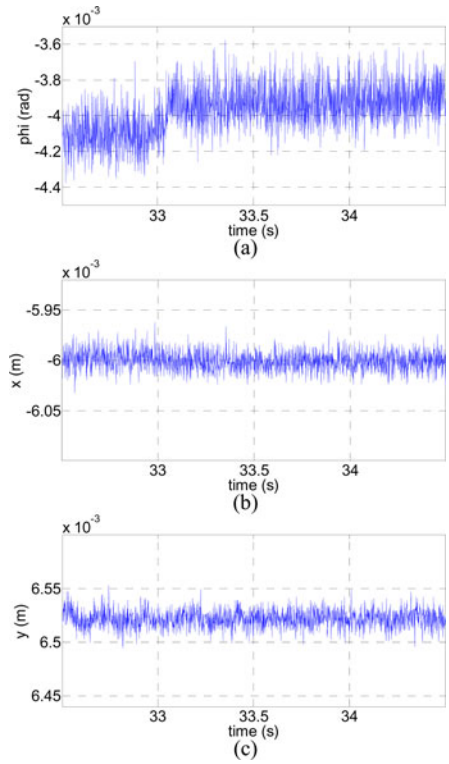

Fig. 18. (a) Step response of 200 μrad in φ and perturbations in (b) x and (c) y.

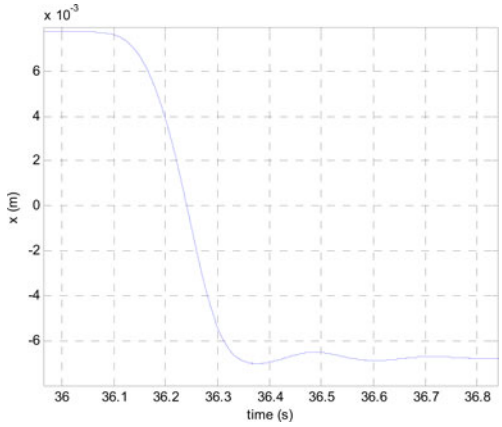

Fig. 19. x-profile of a translational motion in x.

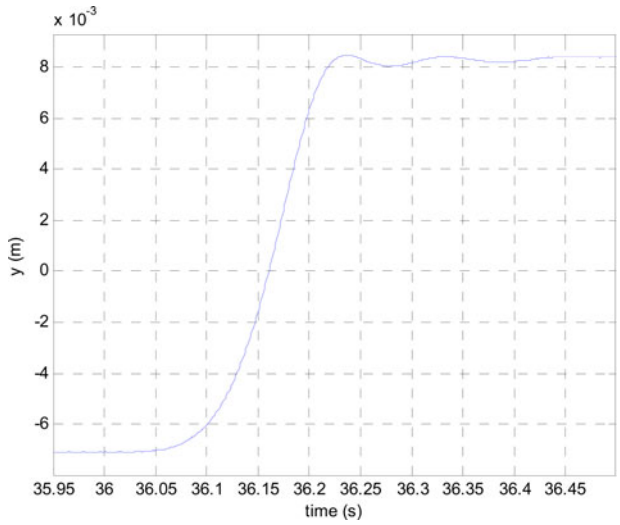

Fig. 20. y-profile of a translational motion in y.

are shown, respectively. The settling time is approximately 1 s, being relatively large. However, no overshoot is exhibited and the steady-state errors are negligibly small. Fig. 18 shows a step response of 200 μrad in rotation about the vertical axis and the perturbations in x and y.

In Fig. 19, the position profile of a motion in x is given. The platen's velocity in x rises from zero to 10.5 cm/s in 0.24 s with an acceleration of 43.8 cm/s^2. Fig. 20 shows the position profile of a motion in y. The platen's velocity rises from zero to 16.3 cm/s in 0.17 s with an acceleration of 95.6 cm/s^2. In this experiment, the maximum magnetic flux density on the surface of $z = 3$ mm, which is generated by the induced Eddy currents in the aluminum spacers, is calculated to be less than 0.06 mT. This is negligibly small in comparison with the 0.7-T peak of the z-direction magnetic flux-density component generated by the superimposed magnet matrix on the surface of $z = 3$ mm. With the maximum currents of 1 A flowing in the coils, the nominal power consumption of the six-coil moving platen is 5.94 W.

VI. Conclusion

In this paper, a 3-DOF planar positioner with a 6-coil single-moving-part platen was designed and constructed to move over a superimposed concentrated-field magnet matrix. Based on the Lorentz force law, the volume integration for force calculation and the electric–current relation for the six-coil platen have been derived. The six coils are divided into three two-phase linear motors. The electromagnetic commutation and the working principle of the moving platen have been verified. The positioner demonstrates a positioning resolution of 8 μm in x and y and 100 μrad in rotation about the vertical axis. The rms positioning error obtained is 6 μm in x and y. Although the design is for the applications that requires 3-DOF planar motions with long travel ranges in x and y and small rotation angles about the vertical axis, the force calculation and the structure of two coils with 270° or 450° phase difference can be utilized for general purposes. This precision planar positioner can be applied as a linear translator or multiaxis mover in which each motor is a forcer generating two independent force components.

References

[1] T. Asakawa, "Two dimensional positioning devices," U.S. Patent 4 626 749, Dec. 1986.
[2] D. L. Trumper, W.-J. Kim, and M. E. Williams, "Design and analysis framework for permanent-magnet machines," *IEEE Trans. Ind. Appl.*, vol. 32, no. 2, pp. 371–379, Mar. 1996.
[3] K. Halbach, "Design of permanent multipole magnets with oriented rare earth cobalt material," *Nuclear Instrum. Methods*, vol. 169, no. 1, pp. 1–10, 1980.
[4] D. L. Trumper, W.-J. Kim, and M. E. Williams, "Magnetic array," U.S. Patent 5 631 618, May 20, 1997.
[5] W.-J. Kim. (Jun. 1997). High-precision planar magnetic levitation, Ph.D. dissertation, Massachusetts Institute of Technology, Cambridge, MA. [Online]. Available: http://dspace.mit.edu/handle/1721.1/10419
[6] T.-J. Hu, Design and control of a 6-degree-of-freedom levitated positioner with high precision, Ph.D. dissertation, Mech. Eng. Dept., Texas A&M University, College Station, TX, May 2005.
[7] J. W. Jansen, C. M. M. van Lierop, E. A. Lomonova, and A. J. A. Vandenput, "Magnetically levitated planar actuator with moving magnets," *IEEE Trans. Ind. Appl.*, vol. 44, no. 4, pp. 1108–1115, Jul./Aug. 2008.
[8] H. Yu, Design and control of a compact 6-degree-of-freedom precision positioner with Linux-based real-time control, Ph.D. dissertation, Mech. Eng. Dept., Texas A&M University, College Station, TX, Aug. 2009.
[9] A. Chitayat, "Two-axis motor with high density magnetic platen," U.S. Patent, 5 777 402, Jul. 1998.
[10] H.-S. Cho, C.-H. Im, and H.-K. Jung, "Magnetic field analysis of 2-D permanent magnet array for planar motor," *IEEE Trans. Magn.*, vol. 37, no. 5, pp. 3762–3766, Sep. 2001.
[11] B. A. Sawyer, "Magnetic positioning device," U.S. Patent 3 376 578, Apr. 2, 1968.
[12] H.-S. Cho and H.-K. Jung, "Effect of coil position and width on back-EMF constant of permanent magnet planar motors," in *Proc. IEEE Int. Electr. Mach. Drives Conf.*, 2001, pp. 430–435.
[13] H.-S. Cho and H.-K. Jung, "Analysis and design of synchronous permanent-magnet planar motors," *IEEE Trans. Energy Convers.*, vol. 17, no. 4, pp. 492–499, Dec. 2002.
[14] V. H. Nguyen. (May 2011). A multi-axis compact positioner with a 6-coil platen moving over a superimposed Halbach magnet matrix, M.S. thesis, Texas A&M University, College Station, TX. [Online]. Available after May 2012: http://hdl.handle.net/1969.1/ETD-TAMU-2011-05-9068
[15] W.-J. Kim, N. D. Bhat, and T. Hu, "Integrated multidimensional positioner for precision manufacturing," *J. Eng. Manuf.*, vol. 218, no. 4, pp. 431–442, Apr. 2004.

Vu Huy Nguyen (S'05) received the B.S. degree in mechanical engineering from the Hanoi University of Technology, Hanoi, Vietnam, in 2005, and the M.S. degree in mechanical engineering from Texas A&M University, College Station, in 2011.

He is currently a lecturer and researcher at University of Transport and Communications, Hanoi, Vietnam. His research interests include design and control of electromechanical actuators, magnetic levitation, and precise positioning.

Won-jong Kim (S'89–M'97–SM'03) received the B.S. (*summa cum laude*) and M.S. degrees in control and instrumentation engineering from Seoul National University, Seoul, Korea, in 1989 and 1991, respectively, and the Ph.D. degree in electrical engineering and computer science from the Massachusetts Institute of Technology (MIT), Cambridge, in 1997.

Since 2000, he has been with the Department of Mechanical Engineering, Texas A&M University (TAMU), College Station, where currently he is an Associate Professor. After the Ph.D. degree, he was with SatCon Technology Corporation, Cambridge, MA, for three years. His current research interests include the analysis, design, and real-time control of mechatronic systems, networked control systems, and nanoscale engineering and technology. He is the holder of three U.S. patents on precision positioning systems.

Dr. Kim, was the recipient of the Korean Institute of Electrical Engineers' Student Paper Contest Grand Prize in 1988, Samsung Electronics' Humantech Thesis Gold Prize for his MIT dissertation in 1997, the NASA Space Act Award in 2002, and the 2005 Professional Engineering Publishing Award for the best paper published in 2004 in *Journal of Engineering Manufacture*. He was appointed as a Select Young Faculty Fellow by TAMU College of Engineering and the Texas Engineering Experiment Station twice in 2003 and 2005. He received the BP Teaching Excellence Award by TAMU College of Engineering in 2006 and was the inaugural Holder of the Guef oil/Thomas A. Dietz Career Development Professorship II during 2007–2010. He is Fellow of ASME and Member of Pi Tau Sigma. He is a Technical Editor of the IEEE/ASME TRANSACTIONS ON MECHATRONICS, the *ASME Journal of Dynamic Systems, Measurement and Control,* the *Asian Journal of Control* and the *International Journal of Control, Automation, and Systems*.